Towards the direct numerical simulation of a self-similar adverse pressure gradient turbulent boundary layer flow

J. Soria and V. Kitsios, C. Atkinson, J.A. Sillero, G. Borrell, A.G. Gungar and J. Jimenez

Abstract This paper presents the results of a study of an adverse pressure gradient TBL (APG-TBL) at the verge of sepration and a zero pressure gradient TBL (ZPG-TBL) developing on a flat surface from the same mean inflow conditions using the TBL DNS code of [14, 1]. The APG-TBL DNS uses a modified wall-normal far-

J. Soria
Laboratory For Turbulence Research in Aerospace and Combustion, Department of Mechanical and Aerospace Engineering, Monash University (Clayton Campus), Melbourne, VIC 3800, AUSTRALIA
and
Department of Aeronautical Engineering, King Abdulaziz University, Jeddah 21589, KINGDOM OF SAUDI ARABIA e-mail: julio.soria@monash.edu

V. Kitsios
Laboratory For Turbulence Research in Aerospace and Combustion, Department of Mechanical and Aerospace Engineering, Monash University (Clayton Campus), Melbourne, VIC 3800, AUSTRALIA e-mail: vassili.kitsios@monash.edu

C. Atkinson
Laboratory For Turbulence Research in Aerospace and Combustion, Department of Mechanical and Aerospace Engineering, Monash University (Clayton Campus), Melbourne, VIC 3800, AUSTRALIAe-mail: callum.atkinson@monash.edu

J.A. Sillero
School of Aeronautics, Universidad Politécnica de Madrid, E-28040 Madrid, SPAIN e-mail: sillero@torroja.dmt.upm.es

G. Borrell
School of Aeronautics, Universidad Politécnica de Madrid, E-28040 Madrid, SPAIN e-mail: guillem@torroja.dmt.upm.es

A.G. Gungar
ITU Faculty of Aeronautics and Astronautics, Department of Astronautical Engineering, Maslak 34469 Istanbul, TURKEY e-mail: ayse.gungor@itu.edu.tr

J. Jimenez
School of Aeronautics, Universidad Politécnica de Madrid, E-28040 Madrid, SPAIN e-mail: jimenez@torroja.dmt.upm.es

field APG boundary condition to yield the self-similar APG-TBL. The maximum Reynolds number based on momentum thickness in the present APG-TBL DNS is $Re_{\delta_2} = 6,700$. The results are compared in the light of a self-similar analysis of the mean boundary layer equations.

1 Introduction

Adverse pressure gradient turbulent boundary layer flow (APG-TBL) is in practical applications the norm rather than the exception and includes applications such as the flow over aircraft wings, wind turbine blades, road vehicles, ships, and flow in turbo-machinery and diffusers. The accurate prediction of TBL separation, a direct consequence of APG-TBL flow, remains a significant challenge for engineering design. One of the complexities of the practical applications of APG-TBL is that the pressure gradient is constantly changing in the streamwise direction, as for example in the large eddy simulation of Kitsios et al. [6].

In the present study our aim is to focus our attention on the canonical flow configuration of a self-similar TBL subjected to an APG such that the TBL is at the verge of separation, akin to the configuration in the experimental study of Skate & Krogstad [15]. A self-similar APG-TBL is defined as having a constant ratio of friction velocity, u_τ, to free-stream streamwise velocity, U_∞, and also a constant ratio of pressure velocity, U_P to U_∞ [10].

Previous direct numerical simulations (DNS) of APG-TBL flows include non-self-similar separated flow [3], and self-similar APG-TBL cases at relatively low Reynolds numbers [16] and [8]. In the present study we undertake DNS of a self-similar APG-TBL developing on a flat surface using the TBL DNS code developed by Simens et al. [14] and Borrell et al. [1]. The code has been modified in the wall-normal far-field to implement the APG boundary condition (BC). The maximum momentum based Reynolds number in the present simulations is $Re_{\delta_2} = 6,700$.

2 Self-similar analysis of APG-TBL

The self-similar analysis as it pertains to APG-TBl is briefly reviewed and the necessary conditions for self-similar APG-TBL to exist are presented. These conditions will be tested using the DNS data to investigate which of them are satisfied. We assume the classical Reynolds decomposition of the dependent variables,

$$\begin{aligned} U_i(\underline{x},t) &= \overline{u}_i(\underline{x}) + u_i(\underline{x},t) \\ P(\underline{x},t) &= \overline{p}(\underline{x}) + p(\underline{x},t), \end{aligned} \tag{1}$$

where $\underline{x} = (x,y,z)$, the subscript i refers to the streamwise, x, wall-normal, y and spanwise, z, directions, with respective instantaneous velocity components in these

directions of $U = U_1$, $V = U_2$ and $W = U_3$. The overlined dependent variables denote the ensemble average of the dependent variables. The associated fluctuating components are denoted by (u, v, w). Assuming that the mean flow is two-dimensional, *i.e.*

$$\begin{aligned} \overline{u}_i(\underline{x}) &= \overline{u}_i(x,y) \\ \overline{p}(\underline{x}) &= \overline{p}(x,y), \end{aligned} \tag{2}$$

then the governing equations for the mean flow are the mean two-dimensional boundary layer equations,

$$\begin{aligned} \partial_x \overline{u} + \partial_y \overline{v} &= 0 \\ \overline{u}\,\partial_x \overline{u} + \overline{v}\,\partial_y \overline{u} &= -\tfrac{1}{\rho}\,\partial_x P_e + \partial_x \overline{v^2} - \partial_y \overline{u^2} - \partial_y \overline{uv} + \nu\,\partial_{y,y}\overline{u}, \end{aligned} \tag{3}$$

where $P_e(x)$ is the streamwise mean pressure distribution in the free-stream, which is related to the streamwise free-stream velocity $U_e(x)$ via Bernoulli's equation. ∂_x, ∂_y and $\partial_{y,y}$ represent partial differentiation with respect to the indicated subscripted independent variable.

The self-similar analysis of the mean governing equations follows the approach initially proposed by [18], [17] and with the less restrictive assumptions suggested by [2]. Assuming the ansatz for the dependent variables,

$$\begin{aligned} \overline{u}(x,y) &= U_e(x) + U_0(x)\,f(\eta) \\ \overline{uv}(x,y) &= -R_{uv}(x)\,r_{uv}(\eta) \\ \overline{u^2}(x,y) &= R_{uu}(x)\,r_{uu}(\eta) \\ \overline{v^2}(x,y) &= R_{vv}(x)\,r_{vv}(\eta) \end{aligned} \tag{4}$$

where $U_0(x)$ is a local velocity scale yet to be determined and $\eta \equiv \frac{y}{L_0(x)}$. where $L_o(x)$ is a local length scale also yet to be determined. In (4) $f(\eta)$ represents the self-similar solution, if it exists, while $r_{uv}(\eta)$, $r_{uu}(\eta)$, $r_{vv}(\eta)$ represent the self-similar functions that describe the relevant Reynolds stresses in (3).

The displacement thickness is defined as

$$\delta_1 \equiv \int_0^\infty \left(1 - \frac{\overline{u}(x,y)}{U_e(x)}\right) dy. \tag{5}$$

Substituting the ansatz yields

$$\delta_1 = \left(-\frac{U_0 L_0}{U_e}\right) \int_0^\infty f(\eta)\,d\eta. \tag{6}$$

Without any loss of generality one can define

$$L_0(x) \equiv \frac{U_0\,\delta_1}{U_e} \;\Rightarrow\; \int_0^\infty f(\eta)\,d\eta = -1. \tag{7}$$

the momentum thickness is defined as,

$$\delta_2 \equiv \int_0^\infty \frac{\overline{u}(x,y)}{U_e(x)} \left(1 - \frac{\overline{u}(x,y)}{U_e(x)}\right) dy, \tag{8}$$

which can be shown to be given by,

$$\delta_2 = \delta_1(x) \left[1 + \frac{U_0(x)}{U_e(x)} \int_0^\infty \{f(\eta)\}^2 \, d\eta\right], \tag{9}$$

and yields the following relationship for the shape factor,

$$H \equiv \frac{\delta_1(x)}{\delta_2(x)} = \frac{1}{\left[1 + \frac{U_0(x)}{U_e(x)} \int_0^\infty \{f(\eta)\}^2 \, d\eta\right]}. \tag{10}$$

Substitution of the ansatz (4) into (3) and after some algebra yields the following mean boundary-layer x-momentum equation form

$$\begin{aligned} &\partial_x (U_o U_e) \; f \; + \; \left(\tfrac{U_o \, U_e}{\partial_x \delta_1} - U_o \; \partial_x U_e\right) \; \eta \; f' \;\; + \; \tfrac{1}{2} \; \partial_x \left({U_o}^2\right) \; f^2 \; - \; {U_o}^2 \; \partial_x \left(\mathrm{Log}\left[\delta_1 \, U_e\right]\right) \; F \; f' \\ &\quad = \tfrac{R_{\mathrm{vv}}}{\partial_x \delta_1} \; \eta \; r'_{\mathrm{vv}} \; - \; \tfrac{R_{\mathrm{uu}}}{\partial_x \delta_1} \; \eta \; r'_{\mathrm{uu}} \; + \; \tfrac{R_{\mathrm{uv}}}{\delta_1^*} \; r'_{\mathrm{uv}} \; + \partial_x R_{\mathrm{vv}} \; r_{\mathrm{vv}} - \partial_x R_{\mathrm{uu}} \; r_{\mathrm{uu}} + \tfrac{\nu \, U_o}{{\delta_1^*}^2} \; f'' \end{aligned} \tag{11}$$

where

$$\begin{aligned} \delta_1^*(x) &\equiv \tfrac{\delta_1(x) \, U_e(x)}{U_o(x)} \\ \delta_1'(x) &\equiv \left\{\partial_x \left(\mathrm{Log}\left[\tfrac{U_o(x)}{\delta_1(x) \, U_e(x)}\right]\right)\right\}^{-1}. \end{aligned} \tag{12}$$

Existence of a self-similar solution $f(\eta)$ requires that all x-dependent coefficients are proportional to each other such that their ratios are independent of x, *i.e.* the following relationships must be simultaneously satisfied,

$$\begin{aligned} \tfrac{1}{2} \; \partial_x \left({U_o}^2\right) \qquad &= c_1 \; \partial_x \left(U_o \, U_e\right) \\ \left(\tfrac{U_o \, U_e}{\delta_1'} - U_o \; \partial_x U_e\right) &= c_2 \; \partial_x \left(U_o \, U_e\right) \\ U_o^2 \; \partial_x \left(\mathrm{Log}\left[\delta_1 \, U_e\right]\right) &= c_3 \; \partial_x \left(U_o \, U_e\right) \\ \tfrac{R_{\mathrm{vv}}}{\delta_1'} \qquad &= c_4 \; \partial_x \left(U_o \, U_e\right) \\ \tfrac{R_{\mathrm{uu}}}{\delta_1'} \qquad &= c_5 \; \partial_x \left(U_o \, U_e\right) \\ \tfrac{R_{\mathrm{uv}}}{\delta_1^*} \qquad &= c_6 \; \partial_x \left(U_o \, U_e\right) \\ \partial_x R_{\mathrm{vv}} \qquad &= c_7 \; \partial_x \left(U_o \, U_e\right) \\ \partial_x R_{\mathrm{uu}} \qquad &= c_8 \; \partial_x \left(U_o \, U_e\right) \\ \tfrac{\nu \, U_o}{{\delta_1^*}^2} \qquad &= c_9 \; \partial_x \left(U_o \, U_e\right) \end{aligned} \tag{13}$$

where $c_1, c_2, ..., c_9$ are constants. The first of the conditions in (13) yields

$$U_o(x) = \mathrm{K}\, U_e(x), \text{ where K is a constant,} \tag{14}$$

This implies that the local velocity scale, $U_o(x)$ is proportional to the local streamwise free-stream velocity, $U_e(x)$. Using (14) permits the definition of Λ as proposed by [2]:

$$\begin{aligned} \Lambda &= -\frac{\partial_x(\mathrm{Log}[U_o])}{\partial_x(\mathrm{Log}[\delta_1])} = -\frac{\partial_x(\mathrm{Log}[U_e])}{\partial_x(\mathrm{Log}[\delta_1])} \\ &= \frac{\partial_x P_e}{\rho\, U_e^2\, \partial_x(\mathrm{Log}[\delta_1])} = \left(\frac{U_p}{U_e}\right)^2 \frac{1}{\partial_x \delta_1} \end{aligned} \tag{15}$$

where $U_p = \sqrt{\frac{\delta_1\, \partial_x P_e}{\rho}}$ is known as the pressure velocity [10]. This allows (11) to be written in the following form,

$$\begin{aligned} &\tfrac{2}{K}\Lambda f + \Lambda f^2 - \tfrac{1}{K}(\Lambda - 1)\,\eta\, f' - (\Lambda - 1)\, F\, f' \\ &\qquad = C_{\mathrm{vv}}\,\eta\, r'_{\mathrm{vv}} - C_{\mathrm{uu}}\,\eta\, r'_{\mathrm{uu}} - K\, C_{\mathrm{uv}}\, r'_{\mathrm{uv}} - D_{\mathrm{vv}}\, r_{\mathrm{vv}} + D_{\mathrm{uu}}\, r_{\mathrm{uu}} - K^2\, C_\nu\, f'' \end{aligned} \tag{16}$$

where

$$\begin{aligned} C_{\mathrm{uu}} &= \tfrac{R_{\mathrm{uu}}}{U_o^2} \\ C_{\mathrm{vv}} &= \tfrac{R_{\mathrm{vv}}}{U_o^2} \\ C_{\mathrm{uv}} &= \tfrac{R_{\mathrm{uv}}}{U_o^2\, \partial_x \delta_1} \\ D_{\mathrm{uu}} &= \tfrac{\partial_x R_{\mathrm{uu}}}{U_o^2\, \partial_x(\mathrm{Log}[\delta_1])} \\ D_{\mathrm{vv}} &= \tfrac{\partial_x R_{\mathrm{vv}}}{U_o^2\, \partial_x(\mathrm{Log}[\delta_1])} \\ C_\nu &= \tfrac{-2\nu}{U_o\, \partial_x \delta_1^2} \end{aligned} \tag{17}$$

must all be independent of x for a self-similar solution $f(\eta)$ to exist. Since Λ is a constant, (15) can be integrated to yield the following power-law relationship between the streamwise free-stream velocity and the displacement thickness with the exponent given by $-\Lambda$

$$\begin{aligned} -\Lambda\, \partial_x(\mathrm{Log}[\delta_1]) &= \partial_x(\mathrm{Log}[U_e]) \\ \Longrightarrow U_e(x) &= A\, \delta_1^{-\Lambda}. \end{aligned} \tag{18}$$

This specific relationship is also a consequence of a self-similar flow. Furthermore, it can be shown that if Λ, C_{uu} and C_{vv} are independent of x, then D_{uu} and D_{vv} must also be independent of x. Therefore, only five conditions need to be independent of x to ensure that a self-similar flow exists, *i.e.* Λ, C_{uv}, C_{uu}, C_{vv} and C_ν must be independent of x. These conditions can be the tested in the APG-TBL and ZPG-TBL DNS to establish if a self-similar solution describing the mean flow can exist.

3 Direct numerical simulation details

The DNS code solves the Navier-Stokes equations in a three-dimensional rectangular volume, with constant density, ρ, and kinematic viscosity, ν. A fractional-step method [4, 11] is used to solve the governing equations for the velocity and pressure (P) fields. Fourier decomposition is used in the periodic spanwise direction, with compact finite differences [9] in the aperiodic wall-normal and streamwise directions. The equations are stepped forward in time using a modified three sub-step Runge-Kutta scheme [14].

The code utilises MPI and openMP parallelisation. For each MPI process the physical domain is decomposed into streamwise regions containing all spanwise and wall-normal points. The physical subdomain is further decomposed into wall normal planes for each openMP thread [1]. All spatial derivatives in the spanwise and wall-normal direction can then be calculated with no MPI message passing. To calculate the streamwise derivatives the data is rearranged into streamwise oriented lines [1].

The boundary conditions of the original ZPG-TBL version of the DNS code are as follows. The bottom surface is a flat plate with a no-slip (zero velocity) BC. The spanwise boundaries are periodic. A downstream streamwise normal plane is copied, and mapped to the inlet BC [13] after being appropriately scaled to account for the ZPG-TBL growth. At the wall-normal far-field boundary the spanwise vorticity is zero, and the wall-normal velocity is given by

$$V_{ZPG}(x) = \frac{d\delta_1(x)}{dx} U_{\infty ZPG} \,, \tag{19}$$

where $U_{\infty ZPG}$ is the constant free-stream streamwise velocity, and δ_1 is the displacement thickness [12]. Note that wall-normal far-field wall-normal velocity represents a suction velocity.

The numerical details of the ZPG-TBL and APG-TBL simulations are summarised in table 1. The number of grid points in each of the three flow directions is given by (N_x, N_y, N_z). The extents of the computational domain in the respective directions (L_x, L_y, L_z) are also presented, along with the constant grid spacings in the streamwise (Δx) and spanwise directions (Δz) and the wall-normal grid spacing at the far-field boundary (Δy_∞) and at the wall (Δy_{wall}). Note the APG simulation has a larger wall normal domain (L_y) and more points in this direction (N_y). This is due to the fact that the APG-TBL expands more quickly in the streamwise direction than the ZPG-TBL. In both simulations the Courant number was set to unity. The length scales in table 1 are non-dimensionalised by $\delta_{99,I}$ as viscous scaling is inappropriate for the APG-TBL flow.

Table 1 Numerical details of the APG-TBL and ZPG-TBL DNS.

	$(L_x, L_y, L_z)/\delta_{99,I}$	$N_x \times N_y \times N_z$	$(\Delta x, \Delta y_{wall}, \Delta y_\infty, \Delta z)/\delta_{99,I}$
ZPG	$(850, 40, 71)$	$8193 \times 315 \times 1362$	$(0.10, 0.0027, 0.18, 0.052)$
APG	$(850, 74, 71)$	$8193 \times 500 \times 1362$	$(0.10, 0.0027, 0.18, 0.052)$

3.1 Adverse pressure gradient boundary condition

In order to implement the desired APG on the turbulent boundary layer development an appropriate wall-normal far-field streamwise wall-normal velocity distribution needs to be specified. Since the interest of the present study is the consideration of an APG-TBL at the point of incipient separation, we refer to the work of Mellor & Gibson [10] who found that the free-stream streamwise velocity distribution for incipient separation scales like $U_{\infty APG}(x) \propto x^m$ where $m = -0.23$ and $(u_\tau \to 0)$. The wall-normal far-field streamwise distribution of the wall-normal (suction) velocity $V_{\infty APG}(x)$ can be deduced from $U_{\infty APG}(x)$ using a boundary layer streamfunction solution in the wall-normal far-field region as

$$V_{\infty APG}(x) = -\frac{dU_{\infty APG}(x)}{dx}\left[y_{BC} - \delta_1(x)\right] + \frac{d\delta_1(x)}{dx} U_{\infty APG}(x)\,, \tag{20}$$

where y_{BC} is the wall normal position of the far-field boundary [10]. Note that for the case of a constant streamwise velocity, *i.e.* the ZPG-TBL, (20) becomes equivalent to (19).

The structure of the complete wall-normal far-field BC, $V_\infty(x)$ shown in Fig. 3.1 is as follows. In the APG-TBL DNS, to allow the rescaling necessary for the inlet BC an initial domain of a ZPG-TBL is simulated up until the streamwise position $x_s = 100\delta_{99,I}$, which is located after the recycling plane, by applying $V_{\infty ZPG}(x)$ as defined by (19). Note that $\delta_{99,I}$ is the boundary layer thickness at the inlet. Downstream of the position $x_f = 140\delta_{99,I}$ the wall normal velocity $V_{\infty APG}(x)$ given by (20) is applied at the wall-normal far-field boundary. This results in the desired free-stream deceleration and hence, expansion of the turbulent boundary layer. From x_s to x_f the velocity $V_{\infty APG}(x)$ is gradually introduced using a smoothing function. Finally towards the outflow of the computational domain the wall-normal velocity in the wall-normal far-field transitions from suction $(V_\infty(x) > 0)$ at $x_o = 760\delta_{99,I}$ to blowing $(V_\infty(x) < 0)$ to reduce the number of instantaneous reversed flow events at the outflow boundary conditions and thus maintain the numerical stability of the DNS. The streamwise functional form of the ZPG and APG wall-normal far-field boundary conditions, $V_\infty(x)/U_{\infty,I}$, is shown in Fig. 2, where $U_{\infty,I}$ is the free-stream streamwise velocity at the inlet.

This wall-normal far-field BC was first implemented and tested using two-dimensional Reynolds Averaged Navier Stokes (RANS) simulations, yielding the appropriate self-similar velocity profiles and subsequently implemented in the DNS code.

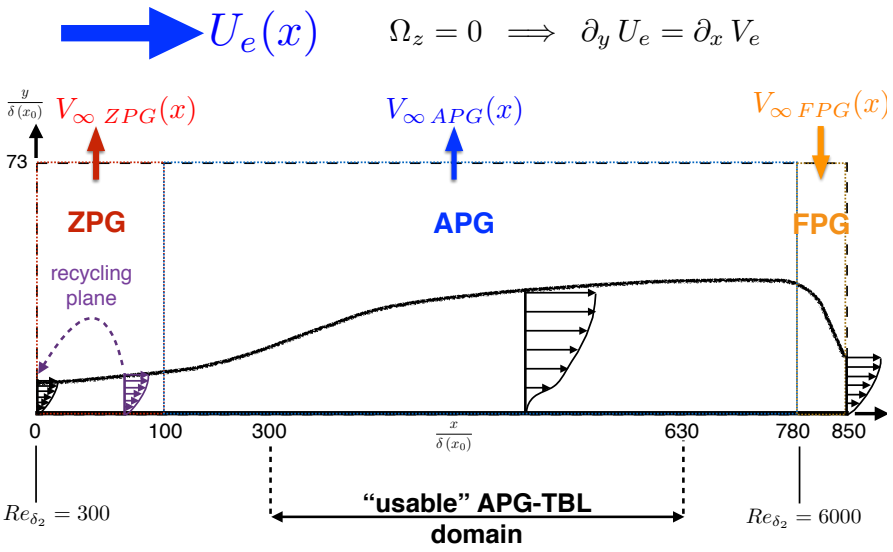

Fig. 1 Schematic of the streamwise wall-normal domain and pertinant parameters of the DNS.

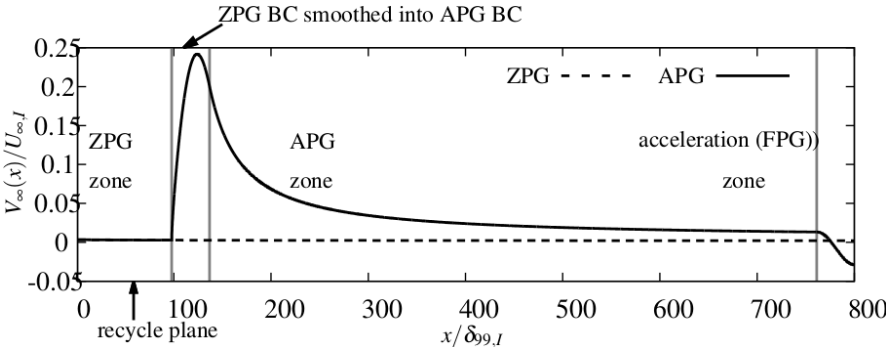

Fig. 2 Far-field wall-normal velocity boundary condition in the adverse pressure gradient (solid line) and zero pressure gradient (dashed line) direct numerical simulation.

4 Results

4.1 Streamwise variation of pertinent parameters

The streamwise variation of Λ, C_{uv}, C_{uu}, C_{vv} and C_ν for the APG-TBL and ZPG-TBL DNS are shown in Fig. 3 for the domain $300 < x/\delta(x_0) < 630$. In this domain of the DNS, Λ, C_{uv}, C_{uu} and C_{vv} are approximately constant for the APG-TBL,

C_V has a slight streamwise decay. In contrast the ZPG-TBL shows a significant streamwsie variation in C_{uv} and C_V. Given these results a self-similar flow for the APG-TBL is only to be expected where viscous effects are negligible, that is in the outer layer of the APG-TBL. The arrows along the x-axis in the Λ figure of Fig. 3 correspond to the streamwise locations where the wall-normal profiles for the data shown in section 4.2 are sampled.

For a self-similar flow (10) implies that $H =$ constant which is shown to be the case for the APG-TBL in the corresponding streamwise variation of H in Fig. 4. The various boundary layer thicknesses are found to vary linearly with streamwise directions as shown in Fig. 4, which is consistent with the constant shape factor. Figure 5 shows the variation of the free-stream velocity, $U_e(x)$, with displacement thickness, $\delta_1(x)$ for the APG-TBL and ZPG-TBL. For a self-similar flow according to (18), the relationship should be a power law with an exponent equal to $-\Lambda$, which as the data in Fig. 5 indicates, is approximately satisfied for the APG-TBL DNS.

4.2 Wall-normal velocity statistics profiles

The mean streamwise velocity profiles for the APG-TBL and ZPG-TBL are shown in Fig. 6. Fig. 6 (a) shows that the mean velocity profile scales with viscous units for the entire profile of the ZPG-TBL, while for the APG-TBL this in not the case. The APG-TBL does not scale in defect form either when the velocity is scaled with the viscous velocity u_τ. However, as Fig. 6 (b) and (d) show, when the APG-TBL mean velocity is scaled with δ_1 and U_e as the self-similar analysis of section 2 indicates is required for a self-similar flow, then the scaled mean velocity profiles collapse across the entire layer including in the viscous layer close to the wall.

Figure 7 (a), (c) and (d) show the tangential Reynolds stress profiles for the APG-TBL and ZPG-TBL scaled in viscous units, which clearly shows the lack of scaling using u_τ and viscosity for the APG-TBL. Figure 7 (b), (d) and (f) show the tangential Reynolds stress profiles scaled by the variables δ_1 and U_e required from the self-similar analysis, showing much better collapse of the scaled profiles across the entire APG-TBL layer.

There are further significant differences between the tangential Reynolds stress profiles of the ZPG-TBL and the APG-TBL. The streamwise Reynolds stress profile has a secondary maximum in the outer layer $y > \delta_1$ in the APG-TBL, which is not present in the ZPG-TBL. The maximum in the wall-normal Reynolds stress profile of the APG-TBL is also located at $y > \delta_1$ in the APG-TBL and is much narrower than the much broader peak in the ZPG-TBL that is located in the inner viscous layer around $y^+ \approx 100$.

The spanwise Reynolds stress profile also has a much larger maximum at $y > \delta_1$ in the APG-TBL, with a small inner maximum near $y \approx 0.1\,\delta_1$. The location of this inner maximum coincides approximately with the location of the maximum in the ZPG-TBL spanwise Reynolds stress profile as shown in Fig. 7 (e).

The shear Reynolds stress profiles for the APG-TBL and the ZPG-TBL DNS are shown in Fig. 8. As in the case with the tangential Reynolds stress profiles, there is no collapse of the APG-TBL data when scaled with viscous variables as shown in Fig. 8 (a). However when the APG-TBL shear Reynolds stress profiles are scaled with δ_1 and U_e, then the collapse is much better as shown in Fig. 8 (b). There is also quite a difference in the shear Reynolds stress distribution between the ZPG-TBL and the APG-TBL. The former has a broad maximum spanning $20 < y^+ < 120$, whereas the latter has a maximum in the outer layer at $y \approx 0.1\,\delta_1$. In the APG-TBL there is also a secondary smaller maximum or plateau in the inner layer at $y \approx 0.1\,\delta_1$, with an inflection point located in the profile between these two locations.

5 Discussion and concluding remarks

The appropriate wall-normal far-field (free-stream) boundary conditions have been developed to simulate a self-similar APG-TBL flow. DNS of a ZPG-TBL and a self-similar APG-TBL, with the latter not yet at the verge of separations, have been carried out. Both simulations were started from the same mean inflow ZPG-TBL conditions. The ZPG-TBL DNS reached a Reynolds number $Re_{\delta_2} \approx 4,107$, which is usable up to $Re_{\delta_2} \approx 4,000$, while the APG-TBL reached a Reynolds $Re_{\delta_2} \approx 6,700$, which is usable up to $Re_{\delta_2} \approx 4,820$.

Analysis of the DNS data base of the APG-TBL shows that the coefficients in the appropriately scaled mean x-momentum boundary layer equations are approximately independent of the streamwise direction, except for the viscous coefficient. This suggests that a self-similar flow, scaled with the local length scale $\delta_1(x)$ and the local velocity scale $U_e(x)$, exists, except possibly in the viscous sublayer. The mean velocity and Reynolds stress profiles scaled by these variables, which show quite good collapse across the entire boundary layer of the APG-TBL, support this notion.

It is pertinent to make a few remarks with respect to "BIG DATA" as the DNS of the APG-TBL presented in this paper clearly falls into this category. Staring with some details regarding the APG-TBL DNS: each restart point in time of the DNS requires four files for the fluid velocity vector field and the pressure, amounting to approximately 90 GB of storage for each instant in time of the simulation. Given that it is desirable to store at least 1000 or possibly more of these statistically independent fields for turbulence structure analysis and to determine the statistical characteristics of the turbulence structures, it is self-evident that the storage requirements for one simulation very quickly reaches requirements in the 100s of TB.

In addition to these storage requirements, the other point that needs to be noted is that this simulation, which is quite typical, was conducted non-locally from where the researchers are located, *i.e.* in this case the majority of the simulation was conducted in Germany using the Supermuc Petascale System in Munich, while the researchers setting up the simulation and monitoring it were located in Melbourne Australia. Furthermore, the DNS fields could not be stored in Germany and had

to be transferred using the internet to Melbourne, Australia using the internet. In this instance this was done using standard *scp* or *rsync* commands. However, better and more parallel methods of international big data movement need to developed and implemented, in particular, if this data is to be shared with national and the international research community as the demand for open access sharing increases. One possible approach is to use BitTorrent peer-to-peer file sharing technology, an example of this approach is BioTorrents [7].

One observation is the necessity to collaborate with computer system scientists on these issues of BIG DATA access around the world and how to design robust and efficient web-portals to allow for BIG DATA access and distributed BIG DATA post-processing and visualisation. It seems that many tools for these operations have already been developed by computer scientists, but what seems to be missing is the implementation within our discipline, due to a lack of awareness and/or knowledge of these on our behave and a lack of awareness and/or knowledge of our requirements by computer scientists. The only way for us to progress on these issues is to make linkages and discuss our BIG DATA issues with the computer scientists - "BIG DATA" is a multi-disciplinary problem.

Acknowledgements

The authors would like to acknowledge the support of this research by the Australian Research Council and European Research Council. The computational resources, which are gratefully acknowledged, were provided by the Australian National Computational Infrastructure supported by the Australian government and the Pawsey Supercomputer Centre supported by the Western Australian and Australian governments and PRACE who is supported by the European Union. Julio Soria gratefully acknowledges the support of an Australian Research Council Discovery Outstanding Researcher Award fellowship.

References

1. Borrell, G., Sillero, J., Jiménez, J.: A code for direct numerical simulation of turbulent boundary layers at high reynolds numbers in BG/P supercomputers. Comp. Fluids **80**, 37–43 (2013)
2. George, W.K., Castillo, L.: Near Wall Turbulent Flows. Elsevier Science Publishers (1993)
3. Gungor, A., Simens, M., Jiménez, J.: Direct numerical simulation of wake-perturbed separated boundary layers. J. Turb **134**, 061,024 (2012)
4. Harrow, F., Welch, J.: Numerical calculation of time-dependent viscous incompressible flow of fluid with free surface. Phys. Fluids **8**(12) (1965)
5. Jiménez, J., Hoyas, S., Simens, M., Mizuno, Y.: Turbulent boundary layers and channels at moderate Reynolds numbers. J. Fluid. Mech. **657**(22), 335–360 (2010)
6. Kitsios, V., Cordier, L., Bonnet, J.P., Ooi, A., Soria, J.: On the coherent structures and stability properties of a leading edge separated airfoil with turbulent recirculation. J. Fluid Mech. **683**, 395–416 (2011)

7. Langille, M., JA, E.: Biotorrents: A file sharing service for scientific data. PLoS ONE **5**(4), e10,071. doi:10.1371/journal.pone.0010,071 (2010)
8. Lee, J.H., Sung, J.: Effects of an adverse pressure gradient on a turbulent boundary layer. Int. J. Heat Fluid Fl. **29**, 568–578 (2008)
9. Lele, S.: Compact finite difference schemes with spectral-like resolution. J. Comput. Phys. **103**, 16–42 (1992)
10. Mellor, G., Gibson, D.: Equilibrium turbulent boundary layers. J. Fluid. Mech. **24**, 225–253 (1966)
11. Perot, J.: An analysis of the fractional step method. J. Comput. Phys. **108**, 51–58 (1993)
12. Sillero, J.: High Reynolds number turbulent boundary layers. Ph.D. thesis, Universidad Politénica de Madrid (2014)
13. Sillero, J., Jiménez, J., Moser, R.: One-point statistics for turbulent wall-bounded at reynolds numbers up to $\delta^+ \approx 2000$. Phys. Fluids **25**, 105,102 (2013)
14. Simens, M.P., Jiménez, J., Hoyas, S., Mizuno, Y.: A high-resolution code for tubulent boundary layers. J. Comp. Phys. **228**, 4128–4231 (2009)
15. Skåre, P., Krogstad, P.A.: A turbulent equilibrium boundary layer near separation. J. Fluid. Mech. **272**, 319–348 (1994)
16. Skote, M., Henningson, D.S., Henkes, R.A.W.M.: Direct Numerical Simulation of Self-Similar Turbulent Boundary Layers in Adverse Pressure Gradients. Flow, Turbulence and Combustion **60**(1), 47–85 (1998)
17. Townsend, A.: The structure of Turbulent Shear Flow. Cambridge University Press (1976)
18. Townsend, A.A.: The structure of the turbulent boundary layer. Mathematical Proceedings of the Cambridge Philosophical Society **47**(02), 375–395 (1951)

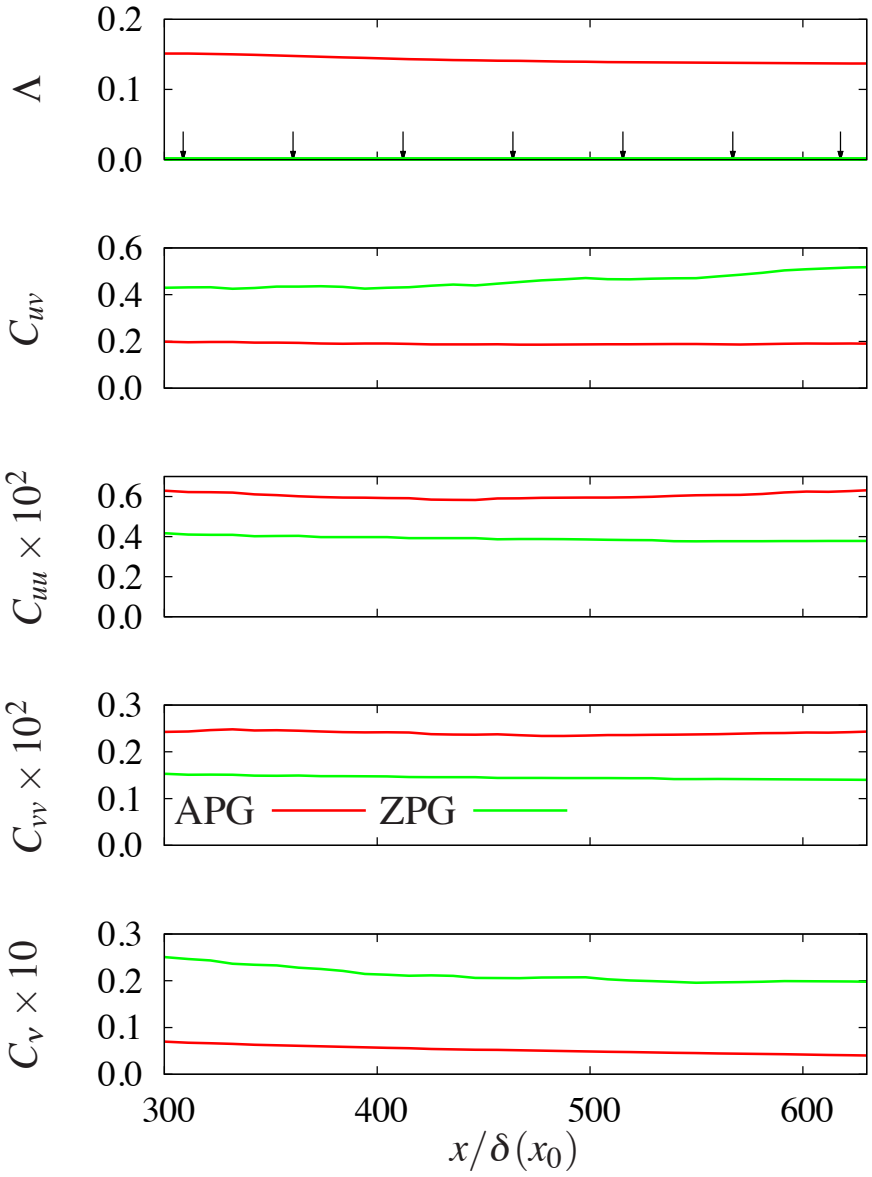

Fig. 3 Streamwise variation of Λ, C_{uv}, C_{uu}, C_{vv} and C_v for the APG-TBL and ZPG-TBL DNS.

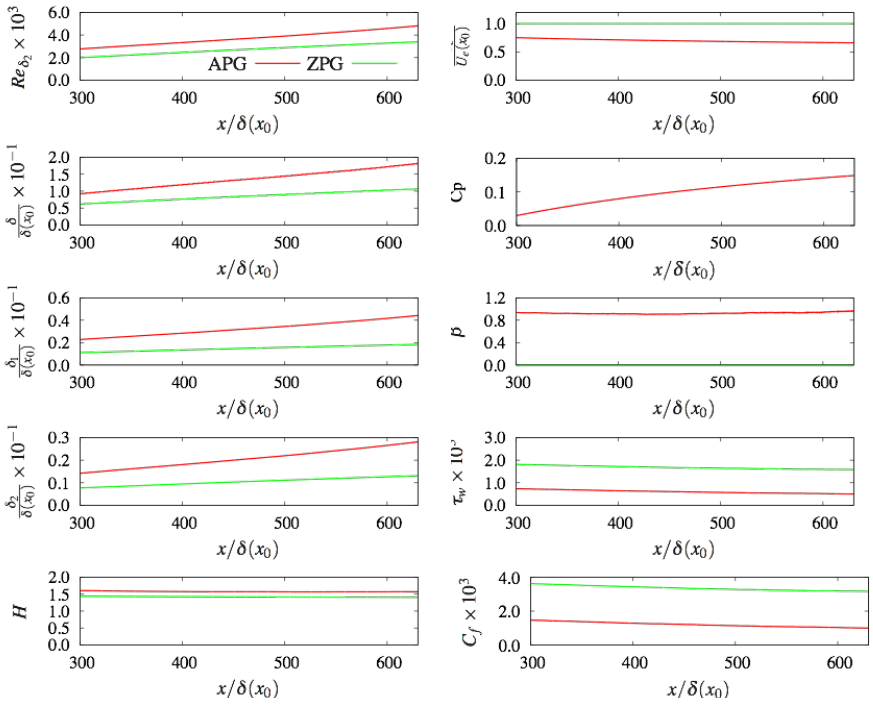

Fig. 4 Variation of boundary layer parameters with streamwise direction for the APG-TBL and ZPG-TBL DNS.

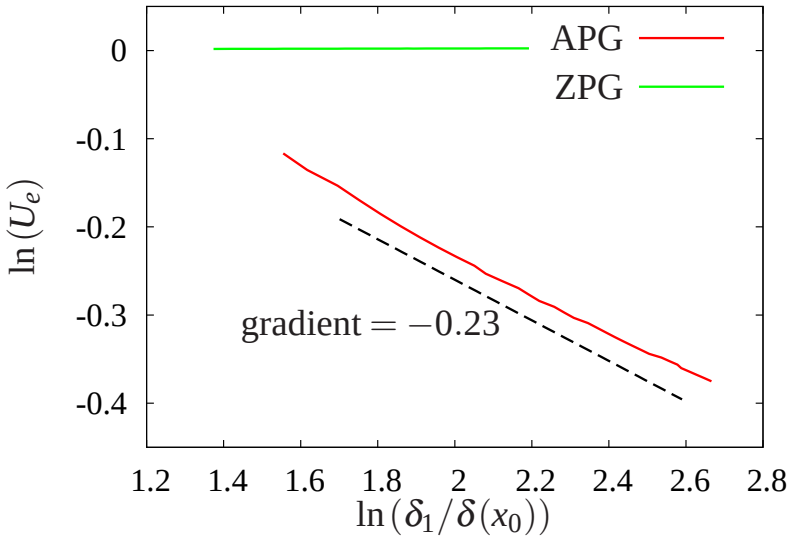

Fig. 5 Variation of free-stream velocity, $U_e(x)$ in with displacement thickness $\delta_1(x)$ for the APG-TBL and ZPG-TBL DNS.

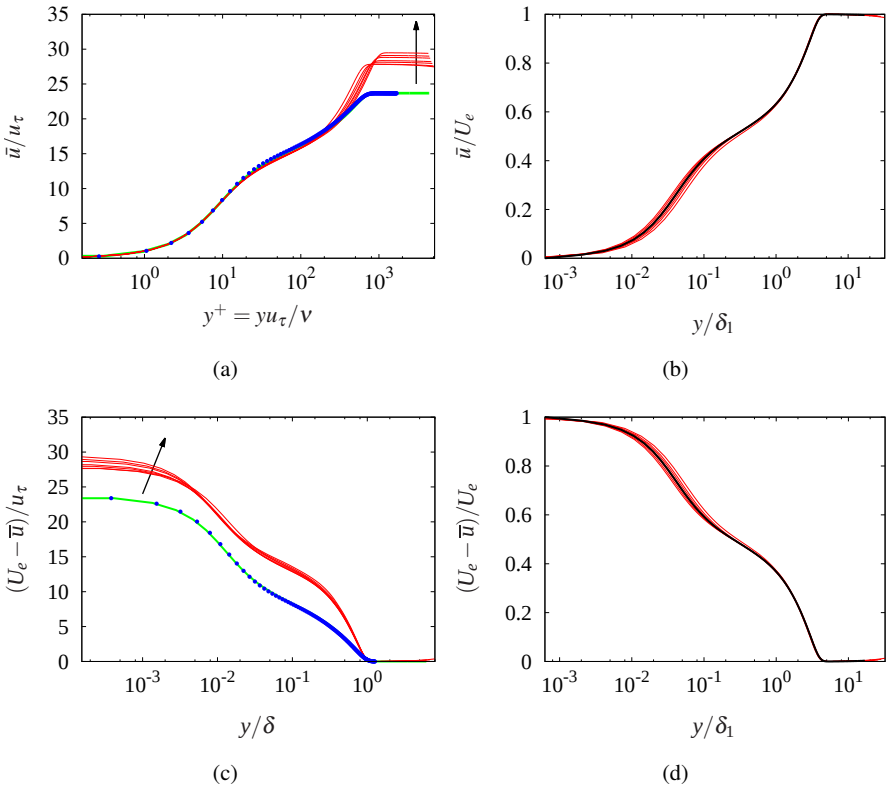

Fig. 6 Streamwise mean velocity profiles, APG-TBL, ZPG-TBL, [5]. (a) and (c) scaled using vsicous units, (b) and (d) scaled using outer scaling using δ_1 and U_e with (c) and (d) plotted in velocity defect form. Note that the black solid line in (b) and (d) represents the average of all profiles shown at the sampling locations indicated in Fig. 3 by the arrows.

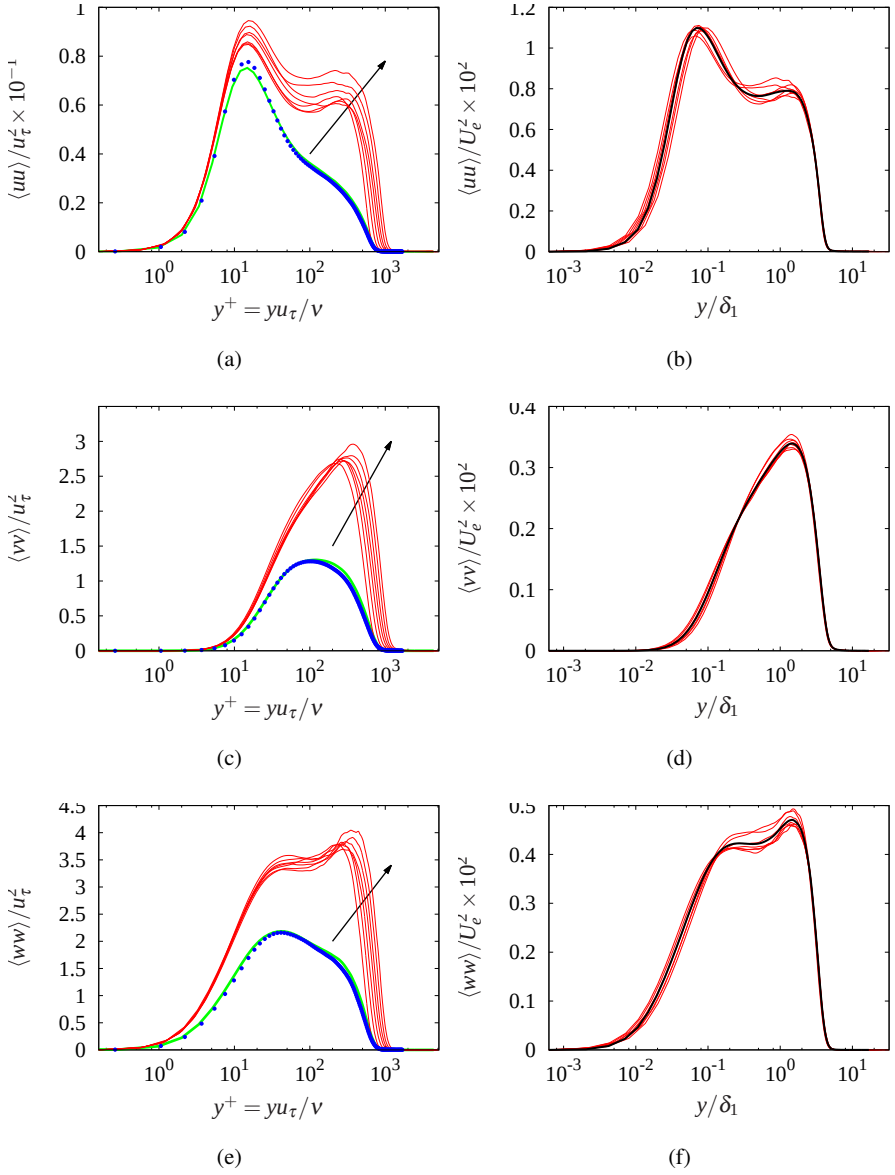

Fig. 7 Tangential Reynolds stress profiles — APG-TBL, — ZPG-TBL, ● [5]. (a), (c) and (e) scaled using viscous units; (b), (d) and (f) scaled using outer scaling using δ_1 and U_e. Note that the black solid line in (b), (d) and (f) represents the average of all profiles shown at the sampling locations indicated in Fig. 3 by the arrows.

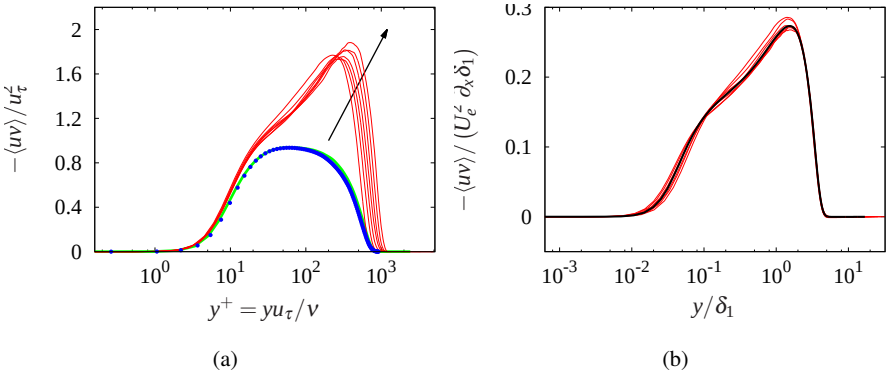

(a) (b)

Fig. 8 Shear Reynolds stress profiles — APG-TBL, — ZPG-TBL, ● [5]. (a) scaled using viscous units; (b) scaled using outer scaling using δ_1 and U_e. Note that the black solid line in (b) represents the average of all profiles shown at the sampling locations indicated in Fig. 3 by the arrows.